PCCP

PAPER

Cite this: *Phys. Chem. Chem. Phys.*, 2016, **18**, 28585

Light-induced charge separation in a P3HT/$PC_{70}BM$ composite as studied by out-of-phase electron spin echo spectroscopy†

Ekaterina A. Lukina,[ab] Alexander A. Popov,[ab] Mikhail N. Uvarov,[a] Elizaveta A. Suturina,[bc] Edward J. Reijerse[c] and Leonid V. Kulik*[ab]

Received 3rd August 2016,
Accepted 20th September 2016

DOI: 10.1039/c6cp05389k

www.rsc.org/pccp

A composite material of semiconducting polymer P3HT and fullerene derivative $PC_{70}BM$ was studied by means of electron spin echo (ESE) spectroscopy. The out-of-phase ESE signal was observed under laser irradiation of the composite at low temperature. We assume that during the charge separation process firstly the spin-correlated radical pairs in the singlet-polarized spin state are formed, and then the net polarization of radical pairs arises due to spin evolution. Both types of polarizations contribute to the out-of-phase ESE signal in the case of non-ideal microwave pulses. Analytical calculation of the echo shape for both types of initial polarization revealed that the contribution of the net polarization becomes zero after averaging over the whole EPR spectrum of the radical pair. This behavior was experimentally confirmed; thus the analysis of the out-of-phase ESE signal was simplified. Interspin distance distributions in the charge transfer state were obtained by modeling the out-of-phase ESE envelope modulation measured at different delays after laser flash T_{DAF} from 300 ns to 3.3 μs at a temperature of 65 K. Due to geminate recombination and diffusion of the radicals from the interface the distribution becomes significantly broader with larger distances prevailing at longer T_{DAF} values. The average distance between charges increases from 3.5 nm to 5.6 nm with an increase in T_{DAF}.

Introduction

The field of organic photovoltaics is rapidly developing.[1–5] Organic solar cells have power conversion efficiencies in the range 8–9%, the largest value obtained so far being 11.2%.[6] This technology already has some commercial applications, but the physics of organic solar cells is still not completely understood. The active layer of bulk heterojunction organic solar cells usually comprises a semiconducting polymer and a fullerene derivative, although new promising materials appear.[7–10] The key process in organic solar sell operation is charge separation under light illumination.[11–13] After the active layer absorbs light, an exciton is formed. It diffuses through the material until it decays to the ground state or reaches the donor–acceptor interface where the electron is transferred from the polymer to the fullerene. Thus the charge transfer (CT) state is formed. Hereafter the CT state separates into free charges with a quantum yield of almost unity for many polymer/fullerene blends.[14,15] Due to the low dielectric constant of organic materials (about 3–4)[16] the Coulomb attraction in the CT state is much higher than the room temperature thermal energy. The understanding of the charge separation mechanism at organic donor/acceptor interfaces still remains a challenge.[17,18] To address this problem knowledge of the structure and properties of the charge-transfer state is required.

Studies dealing with the properties of the short lived charge transfer state in polymer/fullerene systems are scarce. The methods of choice usually are optical spectroscopy[19,20] and time-resolved EPR.[21–27] Time-resolved EPR experiments showed that the CT state is a spin-correlated radical pair (SCRP). The comparison of time-resolved EPR spectra of polymer/fullerene composites and photosynthetic reaction centers revealed that these systems exhibit similar spectra and therefore the charge

[a] *Voevodsky Institute of Chemical Kinetics and Combustion of Siberian Branch of Russian Academy of Sciences, Institutskaya 3, 630090 Novosibirsk, Russia. E-mail: chemphy@kinetics.nsc.ru; Tel: +7-383-3332297*

[b] *Novosibirsk State University, Pirogova 2, 630090 Novosibirsk, Russia*

[c] *Max Planck Institute for Chemical Energy Conversion, Stiftstrasse 34-36, D-45470 Mulheim an der Ruhr, Germany*

† Electronic supplementary information (ESI) available: Details of analytical calculation of time-domain echo shape for singlet and net initial polarizations, figures showing molecular structures of P3HT and $PC_{70}BM$, in-phase and out-of-phase time-domain echo shapes, time-evolution of the out-of-phase echo-detected spectrum, the in-phase echo detected EPR spectrum of P3HT/$PC_{70}BM$ measured with selective microwave pulses, T_1 and T_2 signal decays, out-of-phase ESE signal comparison of the P3HT/$PC_{70}BM$ composite and *Rhodobacter sphaeroides* R26 photosynthetic reaction center, zero-field splitting parameters D and E of the triplet state of fullerene$^-$/polythiophene$^+$ as a function of the distance between their centers and the electron spin density on fullerene$^-$/polythiophene$^+$ calculated by quantum chemistry. See DOI: 10.1039/c6cp05389k

separation mechanisms are supposed to be similar.[25] Recently a powerful tool for spin-correlated radical pair studies – out-of-phase electron spin echo (ESE)[28–30] – has been applied to the benchmark composite of poly(3-hexylthiophene) (P3HT) and fullerene derivative [6,6]-phenyl-C_{61}-butyric acid methyl ester ($PC_{60}BM$).[31] It was shown that the charge transfer state should be described by the distribution of the distance between radicals rather than a fixed distance.[19,31] Also the delocalization of positive charge over several monomers in the polymer chain,[32,33] which is supposed to be an important Coulomb attraction reducing mechanism,[34] should be taken into account. Theoretical consideration of ESE of $P3HT^+/PC_{60}BM^-$ radical pairs revealed that not only singlet-polarized radical pairs but also radical pairs with a net polarization of individual spins can contribute to ESE.[35,36] This polarization is supposed to be acquired due to spin evolution during primary charge separation steps. Another possible contribution to time-resolved EPR and ESE signals is the transfer of the net polarization from the SCRP to the third (observer) spin. In the case of the P3HT/$PC_{60}BM$ blend the $P3HT^+$ or $PC_{60}BM^-$ radicals localized in energy traps can act as the observer spins. The net electron spin polarization transfer can be caused by several mechanisms.[37,38] Among them are (i) the interplay between Zeeman interaction, spin–spin exchange and dipolar coupling in the three-spin system radical pair/observer spin and (ii) doublet–triplet interaction between the observer spin and the triplet that may be formed by radical pair recombination or by intersystem crossing from a singlet exciton. These effects complicate the analysis of time-resolved EPR spectra and in-phase ESE, but usually their influence on out-of-phase echo is not significant.[39]

Here we report on the out-of-phase ESE study of a benchmark composite, containing the polymer P3HT used in the previous study[31] with a different fullerene derivative [6,6]-phenyl-C_{71}-butyric acid methyl ester ($PC_{70}BM$) (molecular structures are shown in Fig. S1, ESI†). $PC_{70}BM$ is a popular fullerene acceptor, widely used in organic photovoltaics.[40–42] Its anion has a wide EPR line[43–45] that simplifies the spin echo shape in the time domain whereas the narrow EPR signal of $PC_{60}BM^-$ complicates the time-domain ESE shape.[31]

In this work we measured the out-of-phase ESE envelope modulation (ESEEM) trace at different times after the laser flash and observed the evolution of the charge transfer state. We determined the interspin distance distribution using the modified model previously proposed for P3HT/$PC_{60}BM$.[31] In addition we showed that the contribution of the net polarization to the out-of-phase echo can be caused by partial selectivity of microwave pulses (non-uniform excitation of the EPR spectrum), and that this contribution disappears after averaging over the whole EPR spectrum of the system.

Theory

Analytical calculation of out-of-phase echo intensity

The Hamiltonian of the radical pair comprises Zeeman interactions of both spins with the external magnetic field and the magnetic interaction between the spins in the radical pair (eqn (1))

$$\hat{H} = \omega_1\hat{S}_{1z} + \omega_2\hat{S}_{2z} + \Gamma\hat{S}_{1z}\hat{S}_{2z}, \quad (1)$$

where $\omega_1 = g_1\beta B_0$ and $\omega_2 = g_2\beta B_0$ are the resonance frequencies of the two radicals, forming the radical pair (g_1 and g_2 are the corresponding g-factors, β is the Bohr magneton, and B_0 is the external magnetic field); Γ is the magnetic interaction between them (the sum of exchange and dipolar interactions). We assumed the weak coupling limit $|\omega_1 - \omega_2| \gg \Gamma$.

The calculation of the echo shape for the pulse sequence α–τ–π–($\tau + t$) (Scheme 1) was performed in the rotating frame using the product operator formalism. The first microwave pulse with length t_p and nominal flip angle α was considered as non-ideal, meaning that the magnetization is rotated around an effective field B_{eff}, which is determined for each radical as $B_{eff(i)} = (B_1,0,B_0 - \omega_0/g_i\beta)$, where B_1 is the amplitude of the microwave field, ω_0 is the frequency of the rotating frame (the microwave frequency), g_i is a g-factor with index i equal to 1 or 2, denoting the radical in the pair, φ_i is the angle between $B_{eff(i)}$ and B_0; in the case of ideal pulses it equals $\pi/2$ meaning that the magnetization is rotated around B_1 under the resonance condition. In the case of non-ideal pulses the magnetization of an individual spin is rotated around the corresponding effective field by an angle $\alpha_i = \alpha|B_{eff(i)}|/B_1$. The interaction between radicals during the first microwave pulse was neglected.

The second microwave pulse was supposed to be ideal, non-selective, and having zero length. The assumption of ideality of the second microwave pulse does not affect the resulting ESE intensity significantly. However, the calculation becomes lengthy with a non-ideal second pulse. We also assumed that the charge recombination and diffusion rates are slow at a low temperature, *i.e.* their characteristic times are much longer than the ESE experiment duration 2τ, therefore all relaxation effects were neglected.

The calculation of echo shapes was performed with initial density matrices $\rho(0) = S_{1z}S_{2z}$ and $\rho(0) = S_{1z}$ describing singlet RP and RP with a net polarization of spin 1, respectively. Note that the term proportional to the unity matrix is omitted in $\rho(0)$. The detailed calculation of the echo intensity can be found in the supporting information.

For singlet initial polarization the out-of-phase echo shape contains both the classical out-of-phase signal[28,46] proportional to $\sin\Gamma\tau$ and also a signal proportional to $\cos\Gamma\tau$. But at time 2τ after the first microwave pulse ($t = 0$) only the signal proportional to $\sin\Gamma\tau$ remains non-zero:

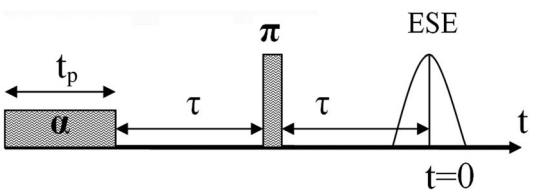

Scheme 1 Pulse sequence used in the calculation.

$$S_x^{\mathrm{SCRP}}(\tau) \propto [\sin\varphi_1 \sin\alpha_1(\sin^2\varphi_2 \cos\alpha_2 + \cos^2\varphi_2) + \sin\varphi_2 \sin\alpha_2(\sin^2\varphi_1 \cos\alpha_1 + \cos^2\varphi_1)]\sin\Gamma\tau \quad (2)$$

In the case of ideal pulses (meaning $\varphi_1 = \varphi_2 = \pi/2$) this expression coincides with that reported elsewhere for weakly interacting spin-correlated radical pairs.[28,46]

We calculated the echo shape for the net initial polarization of spin 1 with the same spin-Hamiltonian (eqn (1)) and obtained that this polarization also produces an out-of-phase ESE signal. At time $t = 0$ this signal exhibits $\cos\Gamma\tau$ dependence which is unusual for the out-of-phase echo:

$$S_x^{\mathrm{net}(1)} \propto \sin\varphi_1 \cos\varphi_1(\cos\alpha_1 - 1)\cos\Gamma\tau \quad (3)$$

This contribution to ESE complicates significantly the determination of the interspin distance in spin-correlated radical pairs from the out-of-phase ESEEM, because this procedure is based entirely on the assumption of $\sin\Gamma\tau$ dependence of the ESE intensity.[28,39] However the term

$$\sin\varphi_i \cos\varphi_i = \frac{(B_0 - \omega_0/g_i\beta)B_1}{(B_0 - \omega_0/g_i\beta)^2 + B_1^2} \quad (4)$$

is antisymmetric with respect to $(B_0 - \omega_0/g_i\beta)$, while the term $(\cos\alpha_i - 1)$ is symmetric. Therefore after averaging over the whole EPR spectrum of the system this signal becomes zero. This is also valid for arbitrary single-spin polarization $\rho(0) = p_1S_{1z} + p_2S_{2z}$.

Thus, in the case of a complex, non-pure singlet initial polarization of radical pairs and non-ideal first microwave pulse, averaging the signal over the whole EPR spectrum of the system will suppress the contribution of the net spin polarization to the out-of-phase ESE. A similar result was recently obtained by numerical modeling for specific initial A/E (absorption/emission) polarization corresponding to $\rho(0) = S_{1z} - S_{2z}$.[36] The singlet spin-correlated radical pair out-of-phase echo does not disappear after field averaging. Its amplitude is proportional to $\sin\Gamma\tau$ and can be used to determine the interspin distance by modeling its dependence on τ.

Experiment

Sample preparation

Regioregular P3HT and $PC_{70}BM$ were purchased from Sigma Aldrich and used without further purification. P3HT and $PC_{70}BM$ (weight ratio 1 : 1) were dissolved in chlorobenzene and mixed using an ultrasonic mixer QSonica Microson XL2000. Several freeze–pump–thaw cycles were performed, after which the solvent was evaporated and the sample tube (o.d. 5 mm or 3 mm) was pumped. Samples were annealed at 10^{-2} Torr and 150 °C for about 10 minutes.

Zn-Substitution of reaction centers of *Rhodobacter sphaeroides* R26 was performed as described in ref. 47. 60–70% v/v final concentration of glycerol was added to protect the sample (quartz tube 4 mm o.d.) from breaking upon cooling.

Pulse EPR experiment

EPR measurements were performed on an X-band EPR spectrometer Bruker ELEXSYS E 580 at the Voevodsky Institute of Chemical Kinetics and Combustion, Novosibirsk, Russia. An ER4118X-MD-5W1 dielectric resonator inside an Oxford ESR 900 cryostat was used. The temperature was set using an Oxford ITC 503 temperature controller and additionally monitored using a Bruker ER4131VT device. A temperature of 65 K was achieved by liquid nitrogen overpumping. In some experiments continuous light irradiation using a halogen lamp was used to observe the light-induced EPR signal in thermal equilibrium. The short-lived CT state in the P3HT/$PC_{70}BM$ composite was created by second harmonic flashes of a Surelite-10 Nd:YAG laser with wavelength 532 nm, flash duration 10 ns, repetition rate 10 Hz, and the incident light intensity on the sample of about 0.6 mJ.

Some measurements were performed at the Max Planck Institute for Chemical Energy Conversion, Mulheim an der Ruhr, Germany, on an X-Band pulse EPR spectrometer Bruker ELEXSYS 580, equipped with an Oxford Instruments CF935 cryostat, an ER 4118X-MS3 split-ring resonator and an ITC4 temperature controller. The temperature was set using liquid helium. Light excitation was realized using an Innolas laser system (532 nm, flash duration 5 ns, repetition rate 10 Hz, 1 mJ light intensity reaching the sample).

After the laser flash and a delay T_{DAF} (DAF – delay after flash) the two-pulse microwave sequence α–τ–π–τ-echo was applied to generate the ESE signal. The nominal duration of the non-selective microwave pulses was set to 8 ns and 16 ns, and their amplitude was optimized to maximize the out-of-phase ESE intensity. It should be noted that the real duration of the pulses is shorter due to the finite rise-time of the microwave field in the resonator. Therefore, the turning angle of the first non-selective pulse was smaller than $\pi/2$ (approximately equal to $\pi/4$). This is important for producing out-of-phase echo, since it has zero intensity if the turning angle of the first nonselective pulse exactly equals $\pi/2$.[28,46] In order to suppress resonator ringing and the free induction decay caused by the second microwave pulse a two-step phase cycling was applied, *i.e.* the measurements with positive $(+x)$ and negative $(-x)$ signs of the first microwave pulse were subtracted one from another.

The signal at long $T_{\mathrm{DAF}} = 99$ ms was attributed to long-living species in thermal equilibrium. Therefore this signal was considered as the background and subtracted from the signals at shorter T_{DAF} in order to obtain the flash-induced signal.

During the measurements of the signal evolution with increasing delay between the microwave pulses (ESEEM experiment) a reproducible variation of the ESE phase of instrumental origin was observed. This effect was compensated for by recording the τ dependent phase profile at $T_{\mathrm{DAF}} = 99$ ms and correcting the signals at smaller T_{DAF} with the inverse phase profile. Special care was taken to avoid the irreproducible drift of the ESE phase caused by the drift of the resonator temperature. For this reason the temperature was stabilized at least for 3 hours before measurements. Very similar out-of-phase ESEEM traces were observed using different spectrometers (at Novosibirsk and Muelheim an der Ruhr).

Quantum chemical calculation

We used the ORCA 3.0[48] quantum chemistry computational package for all calculations. The geometry of thiophene polymer

chains was optimized using the BP86 functional,[49,50] with Ahlrichs polarized basis set def2-TZVP[51–53] and Grimme's dispersion correction D3.[54,55] The resolution of the identity approximation was employed with the auxiliary basis set def2-TZVP/J in order to speed up the calculations.[56]

Spin–spin contribution to the zero-field splitting of the triplet state of the radical pair was computed using pure (BP86/def2-SVP) and hybrid (TPSSh/def2-SVP) functionals with the localized orbital approximation that gives similar results to the restricted orbital approximation.[57] Both functionals give similar results for D and E values as a function of the distance between the center of the polythiophene chain and the center of the fullerene.

Results

Time-domain echo shape

The in-phase and out-of-phase time-domain echo shapes of the P3HT/$PC_{70}BM$ composite were analyzed. Fig. S2 and S3 (ESI†) show the signals measured with T_{DAF} 300 ns and 99 ms and their difference corresponding to the flash-induced signal at τ = 120 ns and 400 ns, respectively. The in-phase echo is bell-shaped for both τ values in contrast to the complicated echo shape observed previously for the P3HT/$PC_{60}BM$ composite.[31] An integration gate of 80 ns centered at the maximum of the in-phase echo was chosen for further experiments.

The out-of-phase echo shape at T_{DAF} = 99 ms weakly oscillates while the integrated echo intensity is almost zero for both τ values. At T_{DAF} = 300 ns the signal at τ = 120 ns exhibits a non-symmetric oscillation giving a small positive signal upon time-domain integration; at τ = 400 ns a negative signal related to the spin-correlated radical pair contribution appears.

Echo-detected EPR spectra

We measured field swept spectra of the P3HT/$PC_{70}BM$ composite with delays T_{DAF} = 300 ns and 99 ms between the excitation laser flash and the microwave pulse sequence. Spectra of $P3HT^+$ and $PC_{70}BM^-$ strongly overlap due to the small difference in g-values. However, a small shoulder at the low field side can be identified as part of the $PC_{70}BM^-$ spectrum (Fig. 1a).[43–45] The in-phase flash-induced spectrum has emissive polarization in low fields and very weak absorptive polarization in high fields, similar to previously observed flash-induced spectra in composites of semiconducting polymers and fullerenes.[25,31]

In the imaginary parts of the spectrum at T_{DAF} = 99 ms the signal is approximately zero (Fig. 1b). At T_{DAF} = 300 ns a negative signal appears. We ascribe this signal to the spin-correlated radical pair charge transfer state formed during the charge transfer process. Evolution of this signal with increasing delay T_{DAF} between the laser flash and the microwave pulse sequence is shown in Fig. S4 (ESI†). The spectrum decays uniformly, without any shape changes.

With the selected microwave pulses the absorptive peaks at the higher field in the real part of the spectrum can be seen more clearly (Fig. S5, ESI†) and the out-of-phase signal disappears (data not shown).

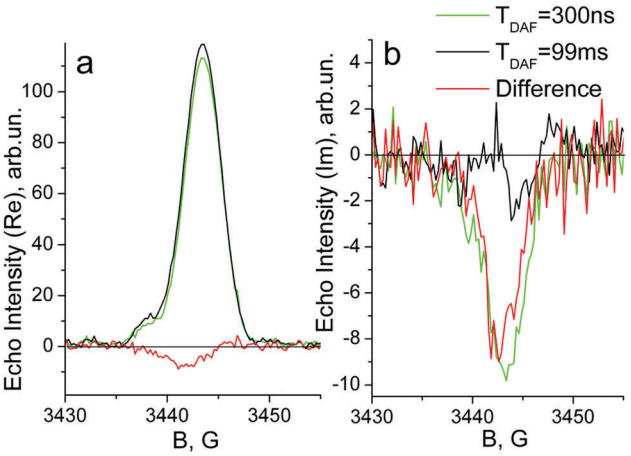

Fig. 1 In-phase (a) and out-of-phase (b) echo detected EPR spectra of P3HT/$PC_{70}BM$ measured at 40 K with T_{DAF} = 300 ns and 99 ms and the flash-induced signal determined as their difference (green, black and red lines respectively). A two-pulse microwave sequence with nonselective pulses and τ = 340 ns was used.

Transient nutations

In order to verify that the out-of-phase ESE signal corresponds to a spin-correlated radical pair, we recorded the spin nutations for both ESE phases using a three-pulse sequence with a varied length of the first pulse. After a 1 μs delay a two-pulse sequence with nonselective pulses and τ = 280 ns was applied for detection. Fig. 2a and b shows the oscillations of the flash-induced signal both in real and imaginary parts of the spectrum. In order to determine the nutation frequency the Fourier transformation was applied (Fig. 2c and d). The time-domain was pretreated with a Gaussian window function of width 0.3 μs

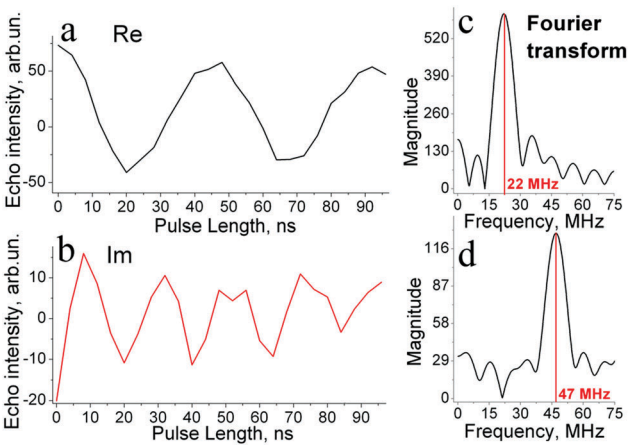

Fig. 2 In-phase (a) and out-of-phase (b) nutation signal of P3HT/$PC_{70}BM$. Flash-induced signals (difference between measurements with T_{DAF} = 300 ns and 99 ms) are shown. A three-pulse microwave sequence was used: the length of the first microwave pulse was varied and subsequently a two-pulse detection sequence with nonselective pulses and τ = 280 ns was applied after the 1 μs delay. Measurements were done at the maximum of the out-of-phase signal (g = 2.0033) at 80 K temperature. The Fourier representation of the in-phase and out-of-phase nutations is presented in panels (c) and (d) respectively.

and subsequently zero-filled to 256 points. This analysis revealed that the out-of-phase ESE oscillation frequency is twice as high as that of the in-phase ESE. This situation corresponds to a spin 1/2 for the in-phase signal and two magnetically coupled correlated spins 1/2 for the out-of-phase signal[59,60] proving our previous suggestion.[31] Note that a similar double frequency nutation (quantum beats) was previously observed in a reaction yield detected magnetic resonance (RYDMR) experiment under spin-locking conditions, and also was consistently explained within the SCRP framework.[61]

Spin relaxation times

We measured relaxation times at 65 K both in the dark and under continuous light illumination by a halogen lamp. T_2 was determined from the ESE decay as a function of the delay between the microwave pulses in the two-pulse sequence α–τ–π. The light-induced signal decays monoexponentially meaning that the T_2 decay times of $P3HT^+$ and $PC_{70}BM^-$ are close to each other and equal approximately 1.5 μs (Fig. S6, ESI†). This time is almost twice as long as the T_2 relaxation time reported for the ESE signal generated by laser flashes in the P3HT/PC_{60}BM composite.[31,58] The dark signal decay with a characteristic decay time of 3.5 μs is much longer than that of the light-induced signal (Fig. S6, ESI†) and cannot be described by exponential decay. The increase of the relaxation rate under light illumination can be caused by a high concentration of radicals.

T_1 was determined from the inversion-recovery experiment with a pulse sequence π–T–$\pi/2$–τ–π. The distribution of T_1 relaxation times is wide, and for light-induced signals there are components with decay times 1.5 μs, 7 μs, 50 μs and 350 μs (Fig. S7, ESI†). The T_1 relaxation time of the dark signal is almost twice longer, and components with decay times 2.5 μs, 10 μs, 100 μs and 700 μs are present (Fig. S7, ESI†). We attribute the wide distribution in longitudinal relaxation times to the strong heterogeneity of the composite and the presence of energetically distributed traps.

The relaxation time and lifetime of flash-induced species were estimated from measurements of ESE evolution with the increase of T_{DAF}. The signal in the real part of the spectrum has an initial rise with a characteristic time of about 2 μs (Fig. 3). We tentatively attribute it to the spin–lattice relaxation of some fraction of flash-generated CT states. The real part T_{DAF}-dependence also has the slow decaying component with characteristic time 30 μs, presumably corresponding to charge recombination. The signal in the imaginary part lives for about 9 μs, which is appreciably longer than that in P3HT/PC_{60}BM at 65 K.[31] This time is the estimation of the charge-transfer state lifetime in P3HT/PC_{70}BM.

Out-of-phase ESEEM

We measured the dependence of the out-of-phase ESE signals on the delay between the microwave pulses for several T_{DAF} values (300 ns, 1.3 μs, 3.3 μs, 99 ms).

The out-of-phase ESE decay measured at the center field (g = 2.0033) (Fig. 4, left) is positive at the smallest τ values, which contradicts the model for the out-of-phase echo of pure singlet radical pairs.[28] We therefore assume that the initial spin

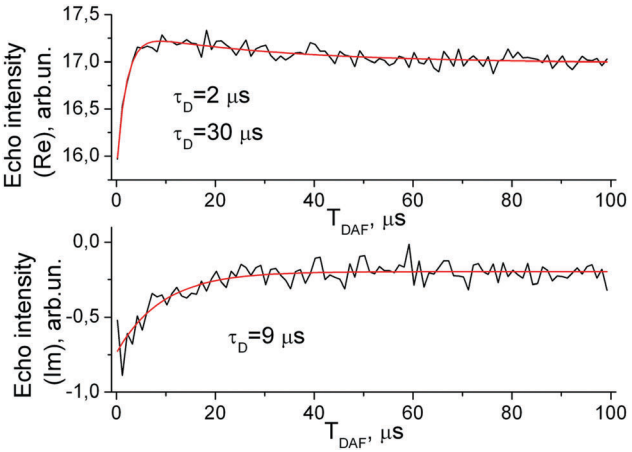

Fig. 3 Signal evolution (upper plot – Re part, lower – Im part) with increasing delay between the laser flash and the microwave pulse sequence. Measurements were done at 65 K at the maximum of the out-of-phase signal (g = 2.0033). The red line represents the bi-exponential fitting with characteristic times 2 μs and 30 μs for the Re part and the exponential fitting with time constant 9 μs for the Im part.

state of the $P3HT^+/PC_{70}BM^-$ radical pair does not have a pure singlet character. Presumably the charge transfer is step-wise, and the primary radical pairs are short-lived; we therefore propose that the radical pairs observed in the ESE experiments are formed after several steps of charge separation, during which the spin polarization is changed.[25] We assume that the ESE signal is formed by spin-correlated radical pairs in which polarization is a superposition of the initial singlet state $\rho(0) = S_{1z}S_{2z}$ and the net polarization $\rho(0) = p_1S_{1z} + p_2S_{2z}$, acquired during spin evolution.[35]

According to the analytical calculation of the echo intensity described above the contribution of the net polarization to the

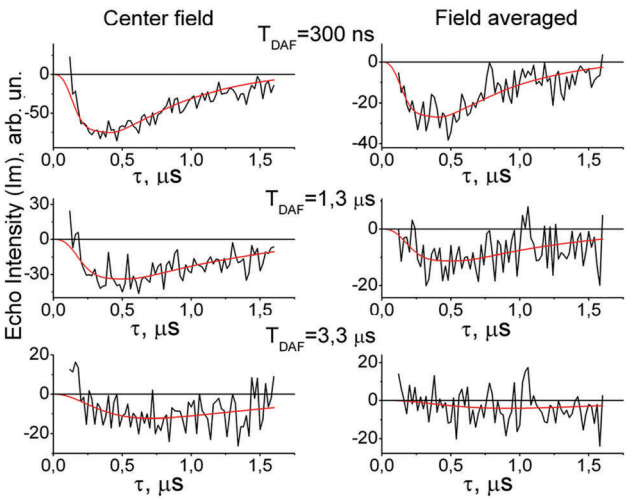

Fig. 4 Out-of-phase (Im) echo evolution with increasing delay between the microwave pulses recorded for different T_{DAF} values at 65 K temperature. Left-side plots were measured at the maximum of the P3HT/PC_{70}BM out-of-phase signal (g = 2.0033); right-side plots represent the field-averaged signal. The red line shows simulation using eqn (6) with distance distributions shown in Fig. 5.

out-of-phase ESE disappears upon averaging over the whole EPR spectrum of the system. This behavior was verified experimentally by averaging the out-of-phase echo evolutions over the 12 G magnetic field range symmetric with respect to the maximum of the out-of-phase echo-detected EPR spectrum. The averaging was done in steps of 0.5 G. After this procedure the non-zero signal at the smallest τ values disappeared and the remaining slow negative component is attributed to the classical out-of-phase signal of singlet radical pairs (Fig. 4, right). The sign of the first oscillation of the out-of-phase echo in the P3HT/$PC_{70}BM$ composite coincides with that of the well-known photosynthetic bacterial reaction center (Fig. S8, ESI†). This was checked by setting the ESE phase for both samples such that the signal under continuous light illumination is in-phase and absorptive-polarized; the out-of-phase signal is zero in this case. Subsequently, the evolutions of the flash-induced out-of-phase echo with increasing delay between the microwave pulses at T_{DAF} = 300 ns were recorded. For both samples the first out-of-phase ESE oscillation is negative. This fact confirms the previously reported similarity between the charge separation process in semiconducting polymer/fullerene blends and photosynthetic reaction centers.[25] This also implies that the out-of-phase ESEEM for both systems is dominated by the dipolar rather than the exchange interaction.

The flash-induced out-of-phase ESEEM in the P3HT/$PC_{70}BM$ composite has a minimum at a τ of about 400 ns at T_{DAF} = 300 ns. With the increase of the delay between the laser flash and the microwave pulse sequence we observed a slight shift of the minimum to longer τ values; also signal evolution slows down. This behavior corresponds to an increase of the distance between the radicals, thus enabling charge separation kinetics analysis.

Discussion

Possible origins of the in-phase ESE signal

Since EPR spectra of $P3HT^+$ and $PC_{70}BM^-$ strongly overlap, unambiguous assignment of the flash-induced emissive in-phase ESE signal seen in Fig. 1a cannot be done. It is possible that spins of both radicals have a net emissive polarization. The net polarization can be formed within the $P3HT^+/PC_{70}BM^-$ SCRP *via* the ST_- mechanism in the case of $J < 0$ or *via* the ST_+ mechanism in the case of $J > 0$ at the initial stage of charge separation, when the strength of the exchange interaction between the radicals is comparable to Zeeman splitting. Some hints for positive J in polymer/fullerene systems were obtained by Kobori *et al.*[22,26] The sign of polarization depends on the initial state and recombination rates for singlet and triplet states of the radical pair.[62]

Alternatively, the emissive ESE signal can originate from the spins of trapped radicals, either $P3HT^+$ or $PC_{70}BM^-$, if charge separation occurs in their vicinity. Such an effect was observed in an artificial donor–acceptor–observer system, in which reversible light-induced charge separation with SCRP formation occurs in the donor–acceptor subsystem, and non-equilibrium spin polarization is partly transferred to the observer spin (stable nitroxide radical).[63] Interestingly, enhanced emissive polarization of the nitroxide spin was observed for this case.

The third possible mechanism is the transfer of polarization to the spins of trapped radicals from triplet excitons. Previously, this was observed in time-resolved EPR experiments on chloranil crystals, in which the electron spins of paramagnetic defects were emissively polarized upon laser excitation due to interaction with triplet excitons.[64] However, no triplet EPR signal is detected in ESE and time-resolved EPR experiments on the P3HT/PCBM composite. Therefore, for the system under study this mechanism is unlikely.

Interestingly, dominating net emissive polarization was obtained in time-resolved EPR experiments on PCDTBT/$PC_{60}BM$ and PTB7/$PC_{60}BM$ composites[25] and in ESE experiment on the P3HT/$PC_{60}BM$ composite.[31] Thus, the net emissive polarization of light-induced radicals seems to be a general feature of polymer/fullerene blends, although its origin is unclear at present. A more detailed study is needed to clarify this issue.

Out-of-phase ESEEM modeling

To simulate the τ dependence of the ESE we modified the model proposed for the P3HT/$PC_{60}BM$ composite.[31] The parameters of the dipolar interaction tensor required for spectral modeling were obtained from quantum chemical calculations. To simplify the calculation we represented $PC_{70}BM$ by a C_{60} molecule and P3HT by an 18 unit polythiophene chain without hexyl substituents. It is known that $PC_{70}BM$ has three isomers[40] and for all of them the electron spin density of the anion-radical was found to be non-symmetric in contrast to $PC_{60}BM$.[45] However the peculiarities of the electron spin density distribution on $PC_{70}BM^-$ are not essential, because the orientation of the fullerene molecule with respect to the polymer chain is random and therefore all peculiarities will average out.

The DFT calculations were performed for the first triplet state of the fullerene$^-$/polythiophene$^+$ pair. The total spin population on the fullerene$^-$ is the same as that on the polythiophene$^+$ (0.5) for distances larger than 10 Å, and the sum of Mulliken charges is +1 on polythiophene and −1 on fullerene, corresponding to the charge transfer state. The values of the zero field splitting parameters D and E were calculated as a function of distance between the centers of fullerene and the polythiophene chain (Fig. S9, ESI†). Fig. S10 (ESI†) shows an example of the calculated electron spin density on the $P3HT^+/PC_{70}BM^-$ radical pair at a distance of 3 nm between the fullerene molecule and the polymer chain.

When the zero field splitting parameters D and E of the dipolar interaction tensor are known, the dipolar frequency can be calculated:

$$\omega_D = 2\pi\left(\frac{2D}{3}\left(1 - 3\cos^2\theta\right) + 2E\sin^2\theta\cos\varphi\right) \qquad (5)$$

where θ and φ are, respectively, the polar and azimuthal angles of the magnetic field B_0 in the reference frame determined by the principal axes of the D tensor. We assume that ω_D is constant during the τ dependence measurements, *i.e.* charge hopping is

slow on the experimental timescale. Also a distance distribution $G(r)$ is taken into account because of the intrinsic disorder of bulk heterojunction blends. Within this model the out-of-phase ESE intensity $M_x(\tau)$ can be calculated by averaging over the distance distribution and orientation angles of the system with respect to the external magnetic field:

$$M_x(\tau) = e^{-2\tau/T_2}\int G(r)\left(\int \sin[\omega_D(\theta,\varphi,r)\tau]\sin\theta d\theta d\varphi\right)dr \quad (6)$$

Eqn (6) is valid for arbitrary shape of the EPR spectrum of the spin correlated radical pair if it is excited uniformly by microwave pulses. T_2 = 2 μs was estimated from the in-phase echo decay of the ESE signal at T_{DAF} = 99 ms (data not shown). Small variations of T_2 do not change the resulting interspin distance distribution significantly.

As the distance distribution $G(r)$ we used a simple model function consisting of two halves of Gaussian distributions: $G(r) = \exp(-(r - r_0)^2/a^2)$ for $r < r_0$, $G(r) = \exp(-(r - r_0)^2/b^2)$ for $r > r_0$. Previously the same distance distribution was employed in the study of the P3HT/$PC_{60}BM$ composite.[31] A similar distribution was used in ref. 19. The Gaussian shape of the distribution is an assumption necessary to simplify fitting, but the model is very sensitive to the position and width of the distribution, therefore the function is not essential. The modeling was done for different T_{DAF} values: 300 ns, 1.3 μs, 3.3 μs.

The fitting was performed for the field-averaged spectra and the interspin distance distribution with the same parameters was applied to describe the signal measured in the center field (Fig. 4). The obtained parameters are listed in Table 1. The center field and field averaged out-of-phase ESEEM spectra differ only for short τ values (less than 200 ns). This is in agreement with the fast decay of the out-of-phase ESE originating from the net polarization of radical pairs.[36] In principle, according to eqn (6), sharp ESEEM features at small τ values can be caused by $P3HT^+/PC_{70}BM^-$ SCRPs with small interspin distances below 2 nm. However, such radical pairs would also produce significant broadening of the time-resolved EPR spectrum of the P3HT/PCBM blend, which was not observed.[21] Analysis of time-resolved EPR linewidth allows the estimation of the lower limit of the charge separation distance of 2.5 nm for the P3HT/$PC_{60}BM$ blend,[25] and a similar limit is expected for P3HT/$PC_{70}BM$. This also justifies the use of the weak spin coupling limit used here for modeling ESEEM traces of $P3HT^+/PC_{70}BM^-$. As can be deduced from Table 1, for the majority of the radical pairs the strength of the dipolar interaction is weaker than 0.5 G, which is much smaller than the width of the EPR spectrum of $P3HT^+/PC_{70}BM^-$. Thus, although the EPR spectra of $P3HT^+$ and $PC_{70}BM^-$ overlap, weak coupling condition breaks only for a small fraction of radical pairs. A similar situation is realized for the SCRP in photosynthetic reaction centers.[28]

Table 1 Interspin distance distribution parameters for different T_{DAF} values, obtained from the simulation of out-of-phase ESEEM traces of $P3HT^+/PC_{70}BM^-$

T_{DAF}	r_0 (nm)	a (nm)	b (nm)	Average distance, r_{av} (nm)
300 ns	2.1	0.3	4.5	3.5
1.3 μs	2.5	0.5	5.9	4.3
3.3 μs	4	2	6	5.6

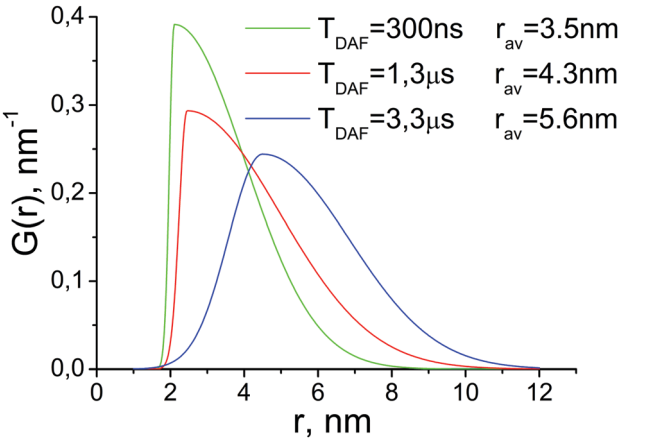

Fig. 5 Distance distributions $G(r)$ between the radicals in the charge transfer state $P3HT^+/PC_{70}BM^-$. Green, red and blue lines represent distributions at T_{DAF} values 300 ns, 1.3 μs and 3.3 μs respectively.

Fig. 5 shows that $G(r)$ depends significantly on T_{DAF} with the average distance r_{av} between charges slightly increasing as T_{DAF} increases; also the distribution becomes significantly broader with larger distances prevailing at longer T_{DAF} values. Two simultaneous processes presumably cause this behavior: diffusion of the radicals from the interface and geminate recombination of radicals that remained close to each other. The low-temperature lifetime of the flash-induced charge-transfer state of the order of several microseconds has been previously measured for artificial fullerene-containing donor–acceptor systems with a distance of 2.8 nm between the charges.[65] Thus, it is likely that the decay of $G(r)$ in the range 2–3 nm with increasing T_{DAF} is caused predominantly by the recombination of CT states.

Previously, the distance between the charges in the charge-transfer state in the P3HT/$PC_{60}BM$ composite was derived from the out-of-phase ESEEM for T_{DAF} = 280 ns and temperature 65 K.[31] A quite small average distance of about 1.5 nm was obtained, which is much shorter than the distances obtained in the present study for a very similar system P3HT/$PC_{70}BM$. This discrepancy is most probably caused by the contribution of the net spin polarization to the out-of-phase ESE which was not taken into account for the case of P3HT/$PC_{60}BM$ in our earlier work.[31] In view of the present results it is clear that the distance between $P3HT^+$ and $PC_{60}BM^-$ was underestimated.

Close to our present results is the distance of initial charge separation of 3–4 nm obtained in the work of Barker *et al.*[19] for the P3HT/$PC_{60}BM$ composite from the analysis of CT state recombination kinetics measured by time-resolved optical absorption spectroscopy for temperatures below 50 K. They also measured the distance in composites of various semiconducting polymers and $PC_{60}BM$ fullerene acceptor with different relative amounts of donor and acceptor compounds and obtained almost the same results for all composites. A 4–6 nm distance

between charges in the CT state was obtained by Gelinas *et al.* at 4 K for the organic BHJ composite consisting of a semiconducting small molecule compound p-DTS(FBTTh$_2$)$_2$ and fullerene PC$_{70}$BM using time-resolved optical electro-absorption spectroscopy on a sub-nanosecond time scale.[20] For both helium and room temperature a very fast initial charge separation step to the distance of about 4 nm was observed, with further moderate increase of this distance.[20] Thus, although charge separation kinetics at donor–acceptor interfaces appears to be complicated, our present results implying initial charge transfer over an appreciable distance of several nanometers are in good agreement with literature data.

Conclusion

The analysis of the out-of-phase ESE signal and transient nutation measurements confirm the spin-correlated nature of the P3HT$^+$/PC$_{70}$BM$^-$ charge transfer state. The signal decay with increasing delay T_{DAF} revealed the estimation of the charge-transfer state lifetime of 10 μs at 65 K. The in-phase ESE signal of P3HT$^+$/PC$_{70}$BM$^-$ is caused by an admixture of the net emissive electron spin polarization. The out-of-phase ESEEM is affected by this net polarization to a certain extent if microwave pulses are not completely nonselective. Analytical calculations of the out-of-phase ESE intensity and shape showed that the contribution of the net polarization becomes zero after averaging over the whole EPR spectrum of the system, while the contribution of the pure singlet spin state to ESE remains nearly unaffected. This behavior was experimentally confirmed. From numerical simulation of the singlet radical pair ESE evolution we obtained the distribution of the distance between the radicals in the CT state of P3HT$^+$/PC$_{70}$BM$^-$. With increasing T_{DAF} from 300 ns to 3.3 μs this distribution becomes significantly broader and the average distance between charges increases from 3.5 nm to 5.6 nm, respectively. Two simultaneous processes are assumed to determine this behavior: diffusion of the radicals from the interface and geminate recombination of radicals that remained close to each other.

Acknowledgements

The authors are thankful to Dr I. I. Proskuryakov (Institute for Basic Biological Problems of the Russian Academy of Sciences, Pushchino) for providing the sample of Zn-substituted of reaction centers of *Rhodobacter sphaeroides* R26 and to Dr A. Savitsky (Max Planck Institute for Chemical Energy Conversion, Mulheim an der Ruhr, Germany) for help during experiments. Elizaveta A. Suturina acknowledges the Russian Foundation for Basic Research for the grant 15-03-03242. The work was also supported by the Russian Foundation for Basic Research grant 15-03-07682a, by the Ministry of Science and Education of Russian Federation, and by the Alexander von Humboldt Foundation research group linkage project ''Light-induced processes and paramagnetic species in organic photovoltaics and photosynthesis''.

References

1 C. Deibel and V. Dyakonov, *Rep. Prog. Phys.*, 2010, **73**, 096401.
2 K. A. Mazzio and C. K. Luscombe, *Chem. Soc. Rev.*, 2015, **44**, 78–90.
3 J. Etxebarria, R. Ajuria and R. Pacios, *Org. Electron.*, 2015, **19**, 34–60.
4 L. Lu, T. Zheng, Q. Wu, A. M. Schneider, D. Zhao and L. Yu, *Chem. Rev.*, 2015, **115**, 12666–12731.
5 X. Liu, H. Chen and S. Tan, *Renewable Sustainable Energy Rev.*, 2015, **52**, 1527–1538.
6 M. A. Green, K. Emery, Y. Hishikawa, W. Warta and E. D. Dunlop, *Prog. Photovoltaics*, 2016, **24**, 905–913.
7 C. B. Nielsen, S. Holliday, H.-Y. Chen, S. J. Cryer and I. McCulloch, *Acc. Chem. Res.*, 2015, **48**, 2803–2812.
8 B. Hemavathi, T. N. Ahipa and R. K. Pai, *Eur. Polym. J.*, 2015, **72**, 309–340.
9 L. Dou, Y. Liu, Z. Hong, G. Li and Y. Yang, *Chem. Rev.*, 2015, **115**, 12633–12665.
10 F. Meyer, *Prog. Polym. Sci.*, 2015, **47**, 70–91.
11 J.-L. Bredas, J. E. Norton, J. Cornil and V. Copopceanu, *Acc. Chem. Res.*, 2009, **42**, 1691–1699.
12 T. M. Clarke and J. R. Durrant, *Chem. Rev.*, 2010, **110**, 6736–6767.
13 C. Deibel, T. Strobel and V. Dyakonov, *Adv. Mater.*, 2010, **22**, 4097–4111.
14 G. Dennler, K. Forberich, M. C. Scharber, C. J. Brabec, I. Tomis, K. Hingerl and T. Fromherz, *J. Appl. Phys.*, 2007, **102**, 054516.
15 J. Jo, S.-I. Na, S.-S. Kim, T.-W. Lee, Y. Chung, S.-J. Kang, D. Vak and D.-Y. Kim, *Adv. Funct. Mater.*, 2009, **19**, 2398–2406.
16 M. Knippera, J. Parisia, K. Coakleyb, C. Waldaufb, C. J. Brabec and V. Dyakonov, *Z. Naturforsch., A: Phys. Sci.*, 2007, **62**, 490–494.
17 F. Gao and O. Inganas, *Phys. Chem. Chem. Phys.*, 2014, **16**, 20291–20304.
18 S. Few, J. M. Frost and J. Nelson, *Phys. Chem. Chem. Phys.*, 2015, **17**, 2311–2325.
19 A. J. Barker, K. Chen and J. M. Hodgkiss, *J. Am. Chem. Soc.*, 2014, **136**, 12018–12026.
20 S. Gelinas, A. Rao, A. Kumar, S. L. Smith, A. W. Chin, J. Clark, T. S. van der Poll, G. C. Bazan and R. H. Friend, *Science*, 2014, **343**, 512–516.
21 J. Behrends, A. Sperlich, A. Schnegg, T. Biskup, C. Teutloff, K. Lips, V. Dyakonov and R. Bittl, *Phys. Rev. B: Condens. Matter Mater. Phys.*, 2012, **85**, 125206.
22 Y. Kobori, R. Noji and S. Tsuganezawa, *J. Phys. Chem. C*, 2013, **117**, 1589–1599.
23 L. Franco, A. Toffoletti, M. Ruzzi, L. Montanari, C. Carati, L. Bonoldi and R. Po, *J. Phys. Chem. C*, 2013, **117**, 1554–1560.
24 F. Kraffert, R. Steyrleuthner, S. Albrecht, D. Neher, M. C. Scharber, R. Bittl and J. Behrends, *J. Phys. Chem. C*, 2014, **118**, 28482–28493.
25 J. Niklas, S. Beaupre, M. Leclerc, T. Xu, L. Yu, A. Sperlich, V. Dyakonov and O. G. Poluektov, *J. Phys. Chem. B*, 2015, **119**, 7407–7416.

26 Y. Kobori and T. Miura, *J. Phys. Chem. Lett.*, 2015, **6**, 113–123.
27 T. Miura, R. Tao, S. Shibata, T. Umeyama, T. Tachikawa, H. Imahori and Y. Kobori, *J. Am. Chem. Soc.*, 2016, **138**, 5879–5885.
28 A. J. Hoff, P. Gast, S. A. Dzuba, C. R. Timmel, C. E. Fursman and P. J. Hore, *Spectrochim. Acta, Part A*, 1998, **54**, 2283–2293.
29 R. Bittl and S. G. Zech, *Biochim. Biophys. Acta, Bioenerg.*, 2001, **1507**, 194–211.
30 W. Lubitz, F. Lendzian and R. Bittl, *Acc. Chem. Res.*, 2002, **35**, 313–320.
31 E. A. Lukina, A. A. Popov, M. N. Uvarov and L. V. Kulik, *J. Phys. Chem. B*, 2015, **119**, 13543–13548.
32 S. A. Holdcroft, *Macromolecules*, 1991, **24**, 4834–4838.
33 J. Niklas, K. L. Mardis, B. P. Banks, G. M. Grooms, A. Sperlich, V. Dyakonov, S. Beaupre, M. Leclerc, T. Xu, L. Yu and O. G. Poluektov, *Phys. Chem. Chem. Phys.*, 2013, **15**, 9562–9574.
34 C. Deibel, T. Strobel and V. Dyakonov, *Phys. Rev. Lett.*, 2009, **103**, 036402.
35 P. J. Hore, *Mol. Phys.*, 1996, **89**, 1195–1202.
36 A. A. Popov, E. A. Lukina, L. L. Rapatsky and L. V. Kulik, *J. Magn. Reson.*, submitted.
37 P. J. Hore, D. J. Riley, J. J. Semlyen, G. Zwanenburg and A. J. Hoff, *Biochim. Biophys. Acta, Bioenerg.*, 1993, **1141**, 221–230.
38 M. T. Colvin, R. Carmiely, T. Miura, S. Richert, D. M. Gardner, A. L. Smeigh, S. M. Dyar, S. M. Conron, M. A. Ratner and M. R. Wasilevski, *J. Phys. Chem. A*, 2013, **117**, 5314–5325.
39 S. A. Dzuba, P. Gast and A. J. Hoff, *Chem. Phys. Lett.*, 1995, **236**, 595–602.
40 M. M. Wienk, J. M. Kroon, W. J. H. Verhees, J. Knol, J. C. Hummelen, P. A. van Hal and R. A. J. Janssen, *Angew. Chem., Int. Ed.*, 2003, **42**, 3371–3375.
41 J. Y. Kim, K. Lee, N. E. Coates, D. Moses, T. Nguyen, M. Dante and A. J. Heeger, *Science*, 2007, **317**, 222–225.
42 F. Zhang, Z. Zhuo, J. Zhang, X. Wang, X. Xu, Z. Wang, Y. Xin, J. Wang, J. Wang, W. Tang, Z. Xu and Y. S. Wang, *Sol. Energy Mater. Sol. Cells*, 2012, **97**, 71–77.
43 O. G. Poluektov, S. Filippone, N. Martın, A. Sperlich, C. Deibel and V. Dyakonov, *J. Phys. Chem. B*, 2010, **114**, 14426–14429.
44 E. A. Lukina, M. N. Uvarov and L. V. Kulik, *J. Phys. Chem. C*, 2014, **118**, 18307–18314.
45 K. L. Mardis, J. N. Webb, T. Holloway, J. Niklas and O. G. Poluektov, *J. Phys. Chem. Lett.*, 2015, **6**, 4730–4735.
46 C. R. Timmel and P. J. Hore, *Chem. Phys. Lett.*, 1994, **226**, 144–150.
47 L. M. Utschig, S. R. Greenfield, J. Tang, P. D. Laible and M. C. Thurnauer, *Biochemistry*, 1997, **36**, 8548–8558.
48 F. Neese, *Wiley Interdiscip. Rev.: Comput. Mol. Sci.*, 2012, **2**, 73–78.
49 J. P. Perdew, *Phys. Rev. B: Condens. Matter Mater. Phys.*, 1986, **33**, 8822–8824.
50 A. D. Becke, *Phys. Rev. A: At., Mol., Opt. Phys.*, 1988, **38**, 3098–3100.
51 A. Schafer, H. Horn and R. Ahlrichs, *J. Chem. Phys.*, 1992, **97**, 2571–2577.
52 A. Schafer, C. Huber and R. Ahlrichs, *J. Chem. Phys.*, 1994, **100**, 5829–5835.
53 F. Weigend and R. Ahlrichs, *Phys. Chem. Chem. Phys.*, 2005, **7**, 3297–3305.
54 S. Grimme, J. Antony, S. Ehrlich and H. Krieg, *J. Chem. Phys.*, 2010, **132**, 154104.
55 S. Grimme, S. Ehrlich and L. Goerigk, *J. Comput. Chem.*, 2011, **32**, 1456–1465.
56 F. Neese, *J. Comput. Chem.*, 2003, **24**, 1740–1747.
57 S. Sinnecker and F. Neese, *J. Phys. Chem. A*, 2006, **110**, 12267–12275.
58 M. N. Uvarov, A. G. Popov, E. A. Lukina and L. V. Kulik, *J. Struct. Chem.*, 2014, **4**, 644–650.
59 K. Hasbaroni, H. Levanon, J. Tang, M. K. Bowman, J. R. Norris, D. Gust, T. A. Moore and A. L. Moore, *J. Am. Chem. Soc.*, 1990, **112**, 6477–6481.
60 C. R. Timmel, C. E. Fursman, A. J. Hoff and P. J. Hore, *Chem. Phys.*, 1998, **226**, 271–283.
61 V. R. Gorelik, K. Maeda, H. Yashiro and H. Murai, *J. Phys. Chem. A*, 2001, **105**, 8011–8017.
62 A. Osintsev, A. Popov, M. Fuhs and K. Mobius, *Appl. Magn. Reson.*, 2001, **20**, 111–135.
63 R. Carmieli, Q. Mi, A. B. Ricks, E. M. Giacobbe, S. M. Mickley and M. R. Wasielewski, *J. Am. Chem. Soc.*, 2009, **131**, 8372–8373.
64 C. Corvaja, L. France, L. Pasimeni, A. Toffoletti and L. Montanari, *Chem. Phys. Lett.*, 1993, **210**, 355–361.
65 M. Di Valentin, A. Bisol, G. Agostini, P. A. Liddell, G. Kodis, A. L. Moore, T. A. Moore, D. Gust and D. Carbonera, *J. Phys. Chem. B*, 2005, **109**, 14401.